Electron transfer and chloride ligand dissociation in complexes [(C$_5$Me$_5$)ClM(bpy)]$^+$/[(C$_5$Me$_5$)M(bpy)]^n (M = Co, Rh, Ir; n = 2 +, +, 0, −): A combined electrochemical and spectroscopic investigation [1]

Wolfgang Kaim [a,*], Ralf Reinhardt [a], Eberhard Waldhör [a], Jan Fiedler [b]

[a] *Institut für Anorganische Chemie der Universität, Pfaffenwaldring 55, D-70550 Stuttgart, Germany*
[b] *J. Heyrovsky Institute of Physical Chemistry, Academy of Sciences of the Czech Republic, Dolejskova 3, CZ-18223 Prague, Czech Republic*

Abstract

In contrast to the rapid and chemically reversible two-electron ECE' reductive elimination reaction [(C$_5$Me$_5$)ClM(bpy)]$^+$ + 2e$^-$ → (C$_5$Me$_5$)M(bpy) + Cl$^-$, M = Rh or Ir, the analogous cobalt system exhibits two separate one-electron steps (EC + E' process) with a persistent, EPR-spectroscopically characterized cobalt(II) intermediate [(C$_5$Me$_5$)Co(bpy)]$^+$. Within the series of coordinatively unsaturated homologous species (C$_5$Me$_5$)M(bpy), the cobalt derivative exhibits the smallest and the iridium homologue the largest metal(I)-to-bpy electron transfer in the ground state, as evident from electrochemical potentials and long-wavelength absorption data. A comparison within that homologous series indicates why the rhodium system, with its intermediate position, is most suitable for hydride transfer catalysis.

1. Introduction

Catalytic oxidative addition/reductive elimination reactions involving the coordinatively unsaturated intermediates (C$_5$Me$_5$)M(bpy), M = Rh, Ir, have been reported for a number of interesting reactions, particularly involving hydride transfer processes [1–9]. Next to the very elementary reactions of electron and proton transfer, the transfer of a hydride equivalent [10] is a basic but also chemically quite relevant kind of chemical process. Spectroscopic and electrochemical analyses [5,9] of these intermediates reveal an unusually delocalized situation in which the π acceptor ligand 2,2'-bipyridine (bpy) serves as an electron reservoir component, creating an effective oxidation state formulation close to (C$_5$Me$_5$)M^{II}(bpy^{-1}). Not unexpectedly, the iridium complexes exhibited lower reactivity [8] and a higher degree of metal-to-ligand charge transfer in comparison with the rhodium analogues [9,11].

In this paper we wish to report pertinent results for the missing member of the series, i.e. (C$_5$Me$_5$)Co(bpy). In view of the typically larger difference between 3d element systems on one side and their 4d and 5d analogues on the other, we shall point out qualitative and quantitative differences between the Co, Rh and Ir compounds. While the Co(III) precursor complex [(C$_5$Me$_5$)ClCo(bpy)]Cl had been reported by Kölle and Fuss [12], there have not yet been any studies of the reduced form (C$_5$Me$_5$)Co(bpy), although related complexes (C$_5$R$_5$)Co(α-diimine) are known with non-aromatic α-diimine ligands (1,4-diaza-1,3-butadienes [13], tetraaza-1,3-butadienes [14,15]).

2. Results and discussion

2.1. Synthesis and NMR characterization

The reaction of [(C$_5$Me$_5$)ClCo(μ-Cl)]$_2$ with 2,2'-bipyridine in dichloromethane produces purple [(C$_5$Me$_5$) ClCo(bpy)]Cl as described previously [11]. Dissolved in dry THF this Co(III) precursor compound was con-

---

* Corresponding author.
[1] Dedicated to Professor Max Herberhold on the occasion of his 60th birthday.

Table 1
^{1}H NMR chemical shifts δ (ppm) of bpy and complexes

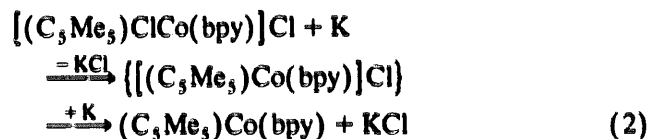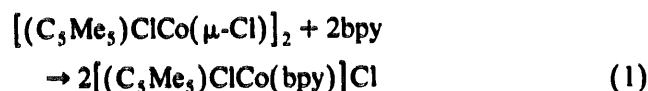| Compound	bpy [a]				(C$_5$Me$_5$)	Solvent
	H^6	H^5	H^4	H^3	CH$_3$	
bpy	8.64	7.33	7.82	8.40	–	CD$_3$CN
[(C$_5$Me$_5$)ClCo(bpy)](Cl)	9.42	7.86	8.22	8.34	1.23	CD$_3$CN
[(C$_5$Me$_5$)ClRh(bpy)](PF$_6$)	8.89	7.81	8.24	8.37	1.65	CD$_3$CN
[(C$_5$Me$_5$)ClIr(bpy)](Cl) [d]	8.88	7.78	8.21	8.44	1.65	CD$_3$CN
(C$_5$Me$_5$)Co(bpy) [b]	10.0 [b]	6.7 [b]	6.7 [b]	6.7 [b]	1.9 [b]	C$_6$D$_6$
(C$_5$Me$_5$)Rh(bpy) [c]	9.10	6.44	6.85	7.45	1.85	C$_6$D$_6$
(C$_5$Me$_5$)Ir(bpy) [d]	8.94	6.16	6.71	7.56	1.75	C$_6$D$_6$

[a] Assignment according to established 2-pyridyl coupling patterns (see Ref. [5]).
[b] Very broad signals ($\Delta\nu_{1/2}$ 70–100 Hz).
[c] Reassigned values from Ref. [5a].
[d] From Ref. [8d].

verted to the extremely air-sensitive and similarly dark purple but better soluble (C$_5$Me$_5$)Co(bpy) through short contact with a freshly prepared potassium mirror. Prolonged contact (more than 5 min) of (C$_5$Me$_5$)Co(bpy) with K results in degradation due to further reduction (see below).

$$[(C_5Me_5)ClCo(\mu\text{-}Cl)]_2 + 2bpy$$
$$\rightarrow 2[(C_5Me_5)ClCo(bpy)]Cl \qquad (1)$$

$$[(C_5Me_5)ClCo(bpy)]Cl + K$$
$$\xrightarrow{-KCl} \{[(C_5Me_5)Co(bpy)]Cl\}$$
$$\xrightarrow{+K} (C_5Me_5)Co(bpy) + KCl \qquad (2)$$

The neutral compound (C$_5$Me$_5$)Co(bpy), as obtained via extraction with benzene, showed severely broadened ^{1}H NMR features (Table 1) but rather normal, narrow ^{13}C NMR signals (Table 2) under the same conditions. Although a paramagnetic impurity cannot be completely ruled out, it is also conceivable that the compound itself has readily accessible excited spin states above the singlet ground state. It was demonstrated before that

pentamethylcyclopentadienide compounds of low-valent 3d metals can exhibit partially populated excited triplet states despite an 18 valence electron configuration [16].

The comparison of ^{1}H NMR data of metal(III) precursors and metal(I) compounds in Table 1 shows a relative low-field shift for H^6 and a high-field shift of the pentamethylcyclopentadienyl protons for the cobalt derivative [(C$_5$Me$_5$)ClCo(bpy)]Cl. These effects reflect the smaller size of the 3d metal cobalt, whereas rhodium and iridium do not differ so much in size due to the lanthanide contraction. The ^{13}C NMR data seem to indicate a special position of (C$_5$Me$_5$)Rh(bpy) in comparison with its homologues, particularly with regard to C^2 and C^5, i.e. the resonances most sensitive to π back-donation.

2.2. Electrochemistry

Both the precursor [(C$_5$Me$_5$)ClCo(bpy)]Cl and the chemically reduced form (C$_5$Me$_5$)Co(bpy) were studied by cyclic voltammetry in acetonitrile (Fig. 1, Table 3). To further investigate the mechanism of chloride dissociation we also applied coulometry and polarography. The cyclic voltammogram of [(C$_5$Me$_5$)ClCo(bpy)]Cl was run in the reduction mode while (C$_5$Me$_5$)Co(bpy) was first oxidized in two steps (Fig. 1). Nevertheless, both cyclic voltammograms in the figure differ only in the first reduction (E_1 vs. $\underline{E}_1$), while the second and third reduction waves are observed at the same potentials (Table 1). Based on previous studies of rhodium and iridium systems [1–9], and in agreement with other electrochemical and spectroscopic results (see below), we propose reaction sequences as given in Schemes 1 and 2. According to these schemes, the neutral compound (C$_5$Me$_5$)Co(bpy) undergoes two reversible one-electron oxidations and one reduction at a very negative potential (Scheme 2). The chlorocobalt(III) precursor shows two relatively close one-electron reductions, the

Table 2
^{13}C NMR chemical shifts δ (ppm) of bpy and complexes

Compound	bpy						(C$_5$Me$_5$)	Solvent
	C^2	C^3	C^4	C^5	C^6		C/CH$_3$	
bpy	156.8	121.4	137.2	124.0	149.4		—	CD$_3$CN
[(C$_5$Me$_5$)ClCo(bpy)](Cl)	156.6	125.1	141.4	129.1	155.2		96.3/10.6	CD$_3$CN
[(C$_5$Me$_5$)ClRh(bpy)](PF$_6$)	154.9	124.3	140.9	128.9	152.5		97.9/8.7	CD$_3$CN
[(C$_5$Me$_5$)ClIr(bpy)](Cl) [a]	156.1	124.9	141.1	129.7	152.6		90.4/8.7	CD$_3$CN
bpy	157.5	121.8	137.3	124.4	150.1		—	C$_6$D$_6$
(C$_5$Me$_5$)Co(bpy)	143.7	119.5	123.6	115.7	152.3		84.4/9.9	C$_6$D$_6$
(C$_5$Me$_5$)Rh(bpy) [b]	136.5	120.7	122.8	116.0	149.8		88.9/9.8	C$_6$D$_6$
(C$_5$Me$_5$)Ir(bpy) [b]	141.0	117.6	123.4	115.3	147.9		83.5/9.7	C$_6$D$_6$

[a] From Ref. [8d].
[b] Reassigned values from Ref. [9a].

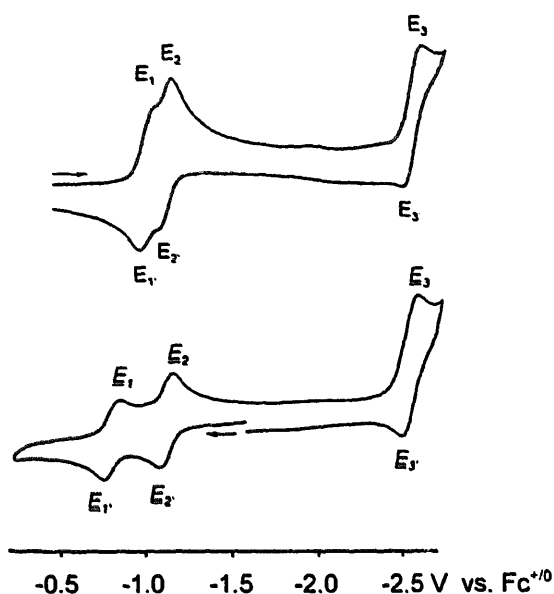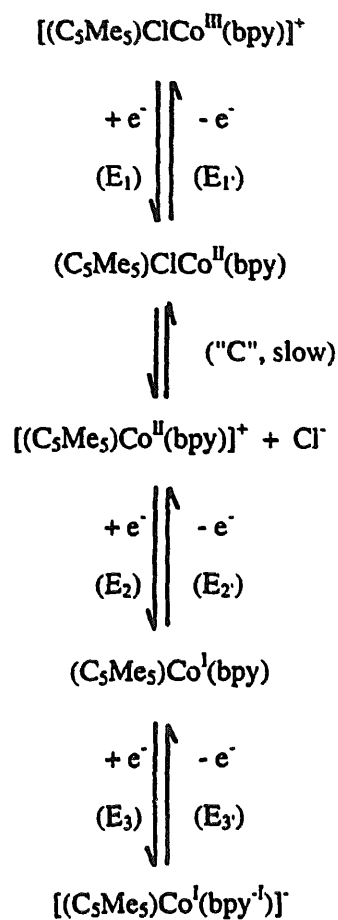Fig. 1. Cyclic voltammograms of [(C₅Me₅)ClCo(bpy)](Cl) (top, 300 mV s⁻¹) and (C₅Me₅)Co(bpy) (bottom, 1000 mV s⁻¹) in CH₃CN + 0.1 M Bu₄NPF₆.

first being sufficient to cause the dissociation of the chloride ligand (chemical step C, Scheme 1).

In order to further substantiate this mechanism we applied polarographic techniques to the reduction behavior of [(C₅Me₅)ClCo(bpy)]Cl. Classical mercury-based polarography [17] can be used to quantify the concentration of free chloride ions in solution due to their strong complexation by mercury ions. According to the Nernst equation, this complex formation lowers the half-wave potential for mercury oxidation. Coulometrically controlled stepwise reduction of [(C₅Me₅)-ClCo(bpy)]Cl revealed (i) that this complex contains one dissociated chloride ion before the reduction, (ii) that the first one-electron reduction produces another equivalent of chloride, signifying labilization of the coordinated chloride and hence an EC mechanism, and (iii) that the second one-electron reduction causes no change in the chloride concentration.

$[(C_5Me_5)ClCo^{III}(bpy)]^+$

$$+e^- \quad\big|\big|\quad -e^-$$
$$(E_1) \quad\quad (E_{1'})$$

$(C_5Me_5)ClCo^{II}(bpy)$

$$\quad\big|\big|\quad (\text{"C", slow})$$

$[(C_5Me_5)Co^{II}(bpy)]^+ \; + \; Cl^-$

$$+e^- \quad\big|\big|\quad -e^-$$
$$(E_2) \quad\quad (E_{2'})$$

$(C_5Me_5)Co^I(bpy)$

$$+e^- \quad\big|\big|\quad -e^-$$
$$(E_3) \quad\quad (E_{3'})$$

$[(C_5Me_5)Co^I(bpy^{-})]^-$

Scheme 1.

Considering Schemes 1 and 2 for the reaction mechanism, it is reasonable to assume that the coordination of σ- and π-donating chloride shifts the potential of the Co(III)/Co(II) step to more negative potentials by 0.18 V (Table 1); in the absence of chloride the Co(III) complex is probably solvated as [(C₅Me₅)(CH₃CN)Co (bpy)]²⁺ [2].

When comparing the cobalt system as reported here with the well-known [1–9] electrochemistry of rhodium

Table 3
Electrochemical potentials E of bpy and complexes [a]

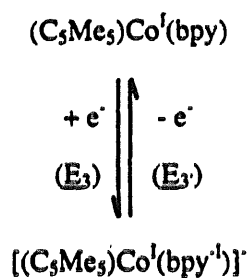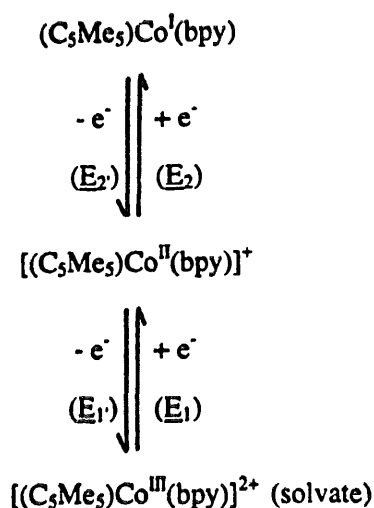| Compound	$E_{1/2}(M^{III/II})$	$E_{1/2}(M^{II/I})$	$E(M^{III/I})$ [b]	$E(M^{I/III})$ [c]	$E_{1/2}(M^{I/0^-})$
bpy					−2.57 [d]
[(C₅H₅)(CH₃CN)Co^{III}(bpy)]⁺ [e]	−0.41	−1.02	—	—	n.r.
(C₅Me₅)Co^I(bpy)	−0.83	−1.15	—	—	−2.56
[(C₅Me₅)ClCo^{III}(bpy)](Cl)	−1.01	−1.15	—	—	−2.56
[(C₅Me₅)ClRh^{III}(bpy)](PF₆)	—	—	−1.36	−1.06	−2.61
[(C₅Me₅)ClIr^{III}(bpy)](PF₆)	—	—	−1.43	−1.08	−2.82

[a] From cyclic voltammetry with 100 mV s⁻¹ scan rate in acetonitrile +0.1 M Bu₄NPF₆. $E_{1/2}$ values with $\Delta E_{pp} = 60$–100 mV. Potentials in volts vs. (C₅H₅)₂Fe⁺/⁰.
[b] Cathodic peak potential for net two-electron reduction.
[c] Anodic peak potential for net two-electron oxidation.
[d] $E_{1/2}(bpy/bpy^{-})$.
[e] From Ref. [19].

$(C_5Me_5)Co^I(bpy)$

$-e^-$ $\Big\Uparrow$ $+e^-$

$(\underline{E}_{2'})$ $\Big|$ $(\underline{E}_2)$

$[(C_5Me_5)Co^{II}(bpy)]^+$

$-e^-$ $\Big\Uparrow$ $+e^-$

$(\underline{E}_{1'})$ $\Big|$ $(\underline{E}_1)$

$[(C_5Me_5)Co^{III}(bpy)]^{2+}$ (solvate)

$(C_5Me_5)Co^I(bpy)$

$+e^-$ $\Big\Uparrow$ $-e^-$

$(\underline{E}_3)$ $\Big|$ $(\underline{E}_{3'})$

$[(C_5Me_5)Co^I(bpy^{-1})]^-$

Scheme 2.

and iridium analogues (Table 3), the most striking difference is the occurrence of a persistent metal(II) form for the 3d system. Both precursor analogues $[(C_5Me_5)ClM(bpy)]Cl$, M = Rh or Ir, are reduced in net two-electron processes with concomitant rapid loss of chloride [1–9]. This reaction could be described within an ECE' mechanism [18] in which E' lies more positive

than E, the effect being a two-electron reductive elimination/oxidative addition. Only under special circumstances, i.e. with sterically hindered α-diimines [9], was the addition reaction associated with reoxidation slowed down so much that intermediates became visible by conventional cyclic voltammetry.

In the cobalt system $[(C_5Me_5)ClCo(bpy)]Cl$, however, E' is slightly more negative than E, so that the EC and E' processes are separated by 0.14 V in the cyclic voltammogram (Fig. 1). This observation illustrates the enhanced stability of the odd-electron state in the 3d metal redox system. Looking at absolute values (Table 3), the cobalt(III) precursor complex is distinctly more easily reduced than the rhodium(III) or iridium(III) analogues, signifying a high degree of additional stabilization for the low-spin d^6 states of the heavier homologues.

2.3. EPR spectroscopy of $[(C_5Me_5)Co(bpy)]^+$

In contrast to the rhodium compounds $(C_5Me_5)Rh(\alpha$-diimine), which yield persistent one-electron oxidized M(II) states only with very strongly π-accepting α-diimine ligands such as 2,2'-azobis(pyridine) (abpy) [20], the cobalt system has now allowed us to study the electrochemically detectable d^7 intermediate $[(C_5Me_5)$-Co(bpy)]^+$ by EPR. The advantageous isotope properties of ^{59}Co (100% natural abundance, $I = 7/2$, high nuclear magnetic moment [21]) may thus be used to investigate the distribution of the unpaired electron. Fig. 2 shows the EPR spectrum of electrochemically generated $[(C_5Me_5)Co(bpy)]^+$ (cf. Eq. (2)) in glassy frozen solution.

Analysis of the EPR spectrum by simulation exhibits a rather "normal" rhombic pattern which had similarly been observed (Table 4) for other half-sandwich complexes [15,22,23], including structurally characterized

Table 4
EPR data of half-sandwich cobalt complexes

Complex	g Components			$\langle g \rangle$ [b]	Δg [c]	$A(^{59}Co)$ [a]			T [d]	Medium
	g_1	g_2	g_3			A_1	A_2	A_3		
closo-(1)Co(TMEDA) [e]	2.549	2.108	1.976	2.224	0.573	2.9	2.7	3.5	4	toluene
$[(C_5Me_5)Co(bpy)]^+$ [f]	2.277	2.094	1.972	2.118	0.305	6.0	2.8	3.0	3.2	CH_3CN
$[(C_5H_5)Co(1,3\text{-}COT)]^-$ [g]	2.196	2.002	1.946	2.051	0.250	4.6	4.1	4.1	153	THF
$[(C_5H_5)Co(1,3\text{-}COD)]^-$ [g]	2.189	≈ 2.0	≈ 2.0	≈ 2.065	≈ 0.19	14.0	≈ 4.2	≈ 4.2	153	THF
$[(C_5H_5)Co(1,4\text{-}Me_2N_4)]$ [h]	2.161	2.022	1.967	2.052	0.194	12.19	1.7	3.0	77	THF

[a] Hyperfine coupling constants (mT).
[b] $\langle g \rangle = [(g_1^2 + g_2^2 + g_3^2)/3]^{1/2}$.
[c] Overall g anisotropy: $\Delta g = g_1 - g_3$.
[d] Temperature (K).
[e] $1 = 2,4\text{-}(SiMe_3)_2\text{-}2,4\text{-}C_2B_4H_4$ (Ref. [22]).
[f] Obtained via electrochemical reduction of $[(C_5Me_5)ClCo^{III}(bpy)](Cl)$ in acetonitrile + 0.1 M Bu_4NPF_6.
[g] From Ref. [23]; COT = cyclooctatetraene, COD = 1,5-cyclooctadiene.
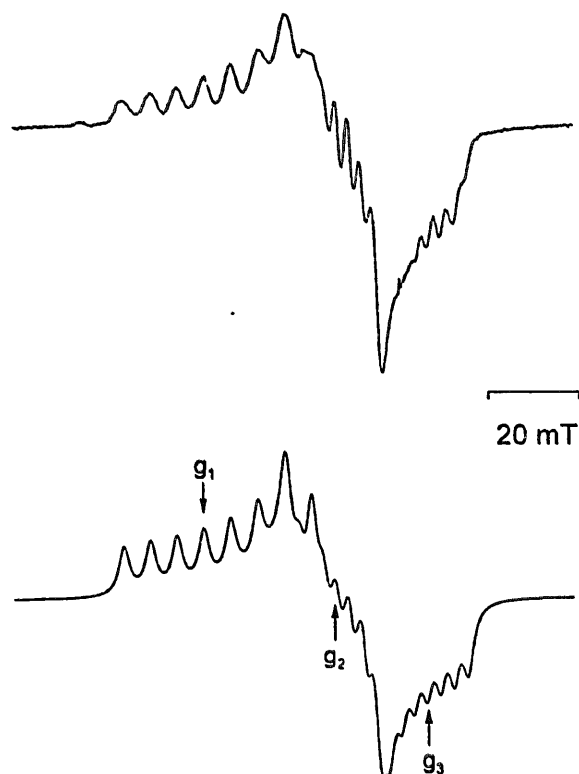[h] From Ref. [15]; $1,4\text{-}Me_2N_4 = 1,4$-dimethyltetraazabutadiene.

Fig. 2. EPR spectrum of electrochemically generated [(C₅Me₅)Co-(bpy)]⁺ at 3.2 K in glassy frozen CH₃CN+0.1 M Bu₄NPF₆ (top) and computer simulation with the data from Table 4 (bottom).

Fig. 3. Absorption spectra of [(C₅Me₅)ClCo(bpy)](Cl) (III), [(C₅Me₅)Co(bpy)]⁺ (II) and (C₅Me₅)Co(bpy) (I) from OTTLE spectroelectrochemistry in CH₃CN+0.1 M Bu₄NPF₆ (absorbance different for each spectrum).

anisotropy, smaller average g values and larger A_1 components. These differences reflect varying degrees of spin delocalization from the metal to the π^* orbital of L, reducing the deviation of g from g(electron) = 2.0023; such deviations have their origins in contributions from higher excited states with non-zero orbital angular momentum, the transition metal cobalt having a much higher spin-orbit coupling constant [21] than the C, N and H nuclei in bpy. In agreement with observations for [(C₅Me₅)Co(R₂N₄)]⁻ anions [14,15], we could not detect a ¹⁴N superhyperfine structure for [(C₅Me₅)Co(bpy)]⁺ (Fig. 2).

neutral closo-1-(TMEDA)-1-Coᴵᴵ-2,4-(SiMe₃)₂-2,4-C₂B₄H₄ [22].

While the dinegative η⁵-carborane ligand in the latter complex is similar to η⁵-C₅Me₅, the saturated TMEDA ligand has no π acceptor capability, in contrast to bpy. According to the EPR parameters in Table 1, the cation [(C₅Me₅)Co(bpy)]⁺ stands between the neutral carborane/TMEDA compound [22] and stronger delocalized anionic systems with better π acceptors; 1,5-cyclooctadiene or 1,4-diaryltetraazabutadienes [15,23]. The increasing π acceptor character of the ligand L in paramagnetic (η⁵-L')CoL species correlates with smaller g
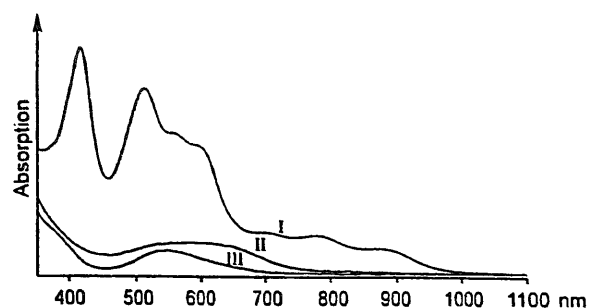
2.4. UV-vis absorption spectroscopy

Following the electrochemical pattern as illustrated in Fig. 1 and summarized in Scheme 2, the stable cobalt complexes [(C₅Me₅)ClCoᴵᴵᴵ(bpy)]⁺, [(C₅Me₅)Coᴵᴵ-(bpy)]⁺ and (C₅Me₅)Coᴵ(bpy) could be observed by spectroelectrochemistry in an optically transparent thin layer electrolysis (OTTLE) cell (Fig. 3) [24]. The starting material and the neutral cobalt(I) compound, synthesized as described in Eq. (2), were studied separately and showed the same spectroscopic features as in the OTTLE experiment, Table 5 summarizes the data.

Table 5
Absorption data of compounds (C₅Me₅)M(bpy) and bpy⁻˙

Compound	λ_{max} (log ε) [a]							$\Delta\nu$ [b]		Solvent
	λ_1			λ_2		λ_3	λ_4			
(C₅Me₅)Co(bpy)	708 (3.28)	790 (3.23)	896 (3.20)	565 (3.83)	602 (3.79)	514 (3.95)	416 (3.97)	1460	1500	n-pentane
(C₅Me₅)Rh(bpy) [c]	682	748	830sh	(sh)	575	516	—	1290	1320	THF
(C₅Me₅)Ir(bpy) [d]	618 π(7) → π(9)	640	740sh	(sh) π(7) → π(10)	533	490	—	1230	1260	n-pentane
bpy⁻˙ [e]	760	843	956	530	564			1300	1400	THF

[a] Wavelengths λ (nm), molar extinction coefficients ε (M⁻¹ cm⁻¹).
[b] Energy differences (cm⁻¹) between the three discernible components of the long-wavelength band.
[c] From Ref. [5a].
[d] From Ref. [9a].
[e] Assignment according to Ref. [24].

The cobalt(III) complex ion $[(C_5Me_5)ClCo(bpy)]^+$ exhibits the typical ligand-field absorptions of an approximately octahedral low-spin d^6 system [25]. There is a moderately intense band in the visible part of the spectrum, assigned to a transition from the $^1A_{1g}$ ground state to the $^1T_{1g}$ excited state. A shoulder at about 380 nm can be assigned to a transition from the $^1A_{1g}$ to the $^1T_{2g}$ state [25]. The spectroelectrochemically generated cobalt(II) cation $[(C_5Me_5)Co(bpy)]^+$, identified by EPR as a low-spin d^7 system, exhibits one very broad feature in the visible region (Fig. 3), probably containing several ligand–field transitions in a low-symmetry situation [25]. The expected absorptions in the near-infrared region could not be established with certainty.

Much more structured and intense absorptions appear when the neutral compound $(C_5Me_5)Co(bpy)$ is generated, either spectroelectrochemically (Fig. 3) or by chemical reduction (Eq. (2)). The absorption spectrum exhibits a basically familiar [5,9,26] pattern for compounds $(C_nR_n)M(bpy)$, i.e. two sets of vibrationally structured long-wavelength absorptions (λ_1, λ_2) and one intense band at about 500 nm (λ_3). In addition, there is an even more intense single band (λ_4) at 416 nm (Fig. 3), which we cannot as yet assign. The vibrational structuring of the two weaker low-energy bands ranges between 1200 and 1500 cm^{-1} and is ascribed [5,9,26,27] to bpy vibrational modes. Similar features are observed for the bpy anion radical [28], which has led us to consider the alternative resonance formulations $(C_5Me_5)M^I(bpy^0) \leftrightarrow (C_5Me_5)M^{II}(bpy^{-1})$ for such neutral species [5,9,26], indicating very strong orbital mixing and metal-to-ligand electron transfer even in the ground state.

The comparison in Table 5 illustrates that the two long-wavelength bands of compounds $(C_5Me_5)M(bpy)$ are shifted to lower energies in the order M = Ir, Rh, Co; however, there is relatively little change in the absorption maximum of the intense λ_3 band around 500 nm. While the low-energy shifts for the cobalt derivative can be understood in terms of the expectedly smaller stabilization of occupied d orbitals relative to those in the rhodium and especially iridium analogue, the intensity and insensitivity of the λ_3 band to metal
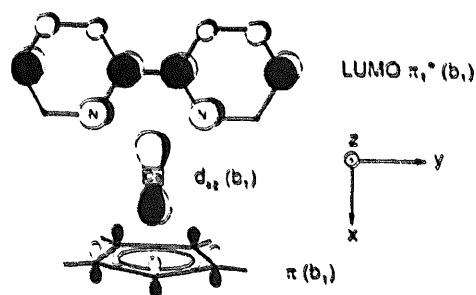
Complex	$E_{1/2}^{ox}$ [c]	$E_{1/2}^{red}$	ΔE [d]	λ_{max}	E_{op} [e]	χ [f]
$(C_5Me_5)Co(bpy)$	−1.15	−2.56	1.41	871	1.42	0.01
$(C_5Me_5)Rh(bpy)$ [g]	−1.09	−2.61	1.52	830	1.49	−0.03
$(C_5Me_5)Ir(bpy)$ [h]	−1.07	−2.82	1.75	720	1.72	−0.03

[a] From cyclic voltammetry in acetonitrile $+0.1$ M Bu_4NPF_6 (see Table 3); potentials in volts.
[b] Absorption maxima λ_{max} (nm) of long-wavelength bands in acetonitrile.
[c] $E_{1/2}^{ox} = E(M^{I/III}) - 0.03$ V for M = Rh, Ir.
[d] $\Delta E = E_{1/2}^{ox} - E_{1/2}^{red}$.
[e] E_{op} (eV); 1 eV $= 8066$ cm^{-1}.
[f] $\chi = E_{op} - \Delta E$.
[g] From Ref. [5a].
[h] From Ref. [9a].

and solvent variation [5] suggest that the underlying transition occurs between highly delocalized orbitals, specifically the π^* MO of 2,2'-bipyridine and the d_{xz} orbital of the metal (Fig. 4). The corresponding transition is then better described as $\pi \rightarrow \pi^*$ between delocalized MOs and not as metal-to-ligand charge transfer (MLCT, $d \rightarrow \pi^*$), which would implicate localized orbitals. Such an assignment would also be supported by MO schemes reported earlier for these and other α-diimine complexes $(C_5R_5)M(\alpha\text{-diimine})$ [5,13–15]. The vibrationally structured lower-energy absorptions are then assigned to less overlap-favored transitions between other d orbitals (e.g. d_{z^2}, d_{yz}) and the lowest π^* MO (b_1) of the bpy ligand (Fig. 4).

The well-resolved absorption spectra and the electrochemical information about compounds $(C_5Me_5)M(bpy)$, M = Co, Rh, Ir invite comparison of both sets of data. To a first approximation [25,29], the energy E_{op} (eV) of the long-wavelength absorption maximum can be compared with the difference ΔE (in V) between
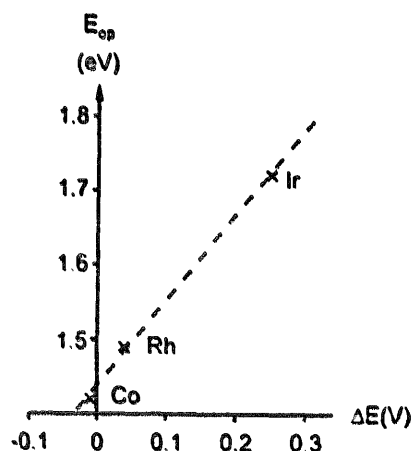

Fig. 4. Metal–ligand orbital interaction in $(C_5Me_5)Co(bpy)$ (b_1 orbitals).

Fig. 5. Correlation between energies E_{op} of the long-wavelength absorption maxima and the differences ΔE between oxidation and reduction potentials of compounds $(C_5Me_5)M(bpy)$. $E_{op} = 1.14\Delta E + 1.44$ eV ($r = 0.999$).

oxidation and reduction potentials. Since E_{op} refers to a "vertical" process (no geometry change during Franck–Condon excitation), while ΔE relates to relaxed states (after geometry reorganization), both figures are connected via the equation $E_{op} = \Delta E + \chi$, where χ summarizes the Franck–Condon contributions from intra- and intermolecular relaxation after excitation [25]. Table 6 contains the pertinent data and Fig. 5 illustrates the correlation between E_{op} and ΔE for all three compounds.

Very small values for χ in Table 6 and the linear correlation in Fig. 5 indicate [29] that the approximation described above is rather good and that there is very little reorganization energy involved. This result confirms the highly delocalized character of the transitions involved ($\pi \rightarrow \pi^*$ rather than MLCT) and is also in agreement with the good resolution (vibrational structuring) of the absorption spectra even at ambient temperatures in solution.

Summarizing the cobalt complexes described here complete the series of analogous rhodium and iridium compounds, confirming established trends but also adding new features such as the stability of an odd-electron ($+$ II) oxidation state. The electrochemical behavior (mechanism, potentials) and the generally lower stability towards dissociation render the cobalt compounds less suitable for the catalysis of hydride transfer, in comparison with both the cobalt and iridium compounds the rhodium system thus exhibits an optimum compromise between stability and catalytic reactivity.

3. Experimental section

3.1. Syntheses

All synthetic and spectroscopic manipulations were carried out under an argon atmosphere using dry solvents.

Compound [(C_5Me_5)ClCo(bpy)](Cl) was obtained according to literature procedures [12,30].

3.1.1. (C_5Me_5)Co(bpy)

50 mg (0.12 mmol) of [(C_5Me_5)ClCo(bpy)](Cl) was suspended in 20 ml of dry THF and brought into contact for 5 min with a freshly distilled potassium mirror (from 40 mg, 1.0 mmol). Filtration, removal of the solvent, extraction with dry benzene and crystallization at -30°C yielded 28 mg (67%) of the extremely air-sensitive dark purple compound. An elemental analysis could thus not be obtained; for spectroscopic data see the main text.

3.2. Instrumentation

EPR spectra were recorded in the X band on a Bruker System ESP 300E equipped with a Bruker

ER035M Gaussmeter and a HP 5350B microwave counter. NMR spectra were taken on Bruker AM 200 and AC 250 spectrometers, infrared spectra were obtained using a Perkin–Elmer 684 instrument. UV/vis/NIR absorption spectra were recorded on Shimadzu UV160 and Bruins Instruments Omega 10 spectrophotometers. Cyclic voltammetry was carried out in dry acetonitrile containing 0.1 M Bu_4NPF_6, using a three-electrode configuration (glassy carbon working electrode, Pt counter electrode, Ag/AgCl reference) and a PAR 273 potentiostat and function generator. The ferrocenium/ferrocene couple served as internal reference. For polarographic measurements we used a multi-purpose polarograph GWP 673. Spectroelectrochemical measurements were performed with an OTTLE cell [24] for UV–vis spectra and a two-electrode capillary for EPR studies [31].

References

[1] U. Kölle and M. Grätzel, Angew. Chem., 99 (1987) 572; Angew. Chem., Int. Ed. Engl., 26 (1987) 568.

[2] U. Kölle, B.-S. Kang, P. Infelta, P. Compte and M. Grätzel, Chem. Ber., 122 (1989) 1869.

[3] S. Cosnier, A. Deronzier and N. Vlachopoulos, J. Ch. ., Soc., Chem. Commun., (1989) 1259.

[4] S. Chardon-Noblat, S. Cosnier, A. Deronzier and N. Vlachopoulos, J. Electroanal. Chem., 352 (1993) 213.

[5] (a) M. Ladwig and W. Kaim, J. Organomet. Chem., 419 (1991) 233; (b) R. Reinhardt and W. Kaim, Z. Anorg. Allg. Chem., 619 (1993) 1998.

[6] R. Reinhardt, J. Fees, A. Klein, M. Sieger and W. Kaim, Wasserstoff als Energieträger, VDI, Düsseldorf, 1994, p. 133.

[7] R. Ruppert, S. Herrmann and E. Steckhan, J. Chem. Soc., Chem. Commun., (1988) 1150; E. Steckhan, S. Herrmann, R. Ruppert, E. Dietz, M. Frede and E. Spika, Organometallics, 10 (1991) 1568; D. Westerhausen, S. Herrmann, W. Hummel and E. Steckhan, Angew. Chem., 104 (1992) 1496; Angew. Chem., Int. Ed. Engl., 31 (1992) 1529; E. Steckhan, S. Herrmann, R. Ruppert, J. Thömmes and C. Wandrey, Angew. Chem., 102 (1990) 445; Angew. Chem., Int. Ed. Engl., 29 (1990) 388.

[8] (a) R. Ziessel, Angew. Chem., 103 (1991) 863; Angew. Chem., Int. Ed. Engl., 30 (1991) 844; (b) R. Ziessel, J. Chem. Soc., Chem. Commun., (1988) 16; (c) R. Ziessel, J. Am. Chem. Soc., 115 (1993) 118; (d) M.-T. Youinou and R. Ziessel, J. Organomet. Chem., 363 (1989) 1987; (e) C. Caix, S. Chardon-Noblat, A. Deronzier and R. Ziessel, J. Electroanal. Chem., 362 (1993) 301.

[9] (a) M. Ladwig and W. Kaim, J. Organomet. Chem., 439 (1992) 79; (b) S. Greulich, W. Kaim, A. Stange, H. Stoll, J. Fiedler and S. Zalis, Inorg. Chem., 35 (1996) 3998.

[10] U. Kölle, New J. Chem., 16 (1992) 157.
[11] W. Bruns, W. Kaim, M. Ladwig, B. Olbrich-Deussner, T. Roth and B. Schwederski, in A.J.L. Pombeiro and J. McCleverty, (eds.) Molecular Electrochemistry of Inorganic, Bioinorganic and Organometallic Compounds, Kluwer, Dordecht, 1993, p. 255.
[12] U. Kölle and B. Fuss, Chem. Ber., 117 (1984) 743.
[13] H. tom Dieck and M. Haarich, J. Organomet. Chem., 291 (1985) 71.
[14] M.E. Gross, W.C. Trogler and J.A. Ibers, Organometallics, 1 (1982) 732; M.E. Gross, W.C. Trogler and J.A. Ibers, J. Am. Chem. Soc., 103 (1981) 192.
[15] M.J. Maroney and W.C. Trogler, J. Am. Chem. Soc., 106 (1984) 4144.
[16] W. Kaim, T. Roth, B. Olbrich-Deussner, R. Gross-Lannert, J. Jordanov and E.K.H. Roth, J. Am. Chem. Soc., 114 (1992) 5693.
[17] A.M. Bond, Modern Polarographic Methods in Analytical Chemistry, Marcel Dekker, New York, 1980.
[18] D. Astruc, Electron Transfer and Radical Processes in Transition-Metal Chemistry, VCH, Weinheim, 1995.
[19] U. Kölle, J. Organomet. Chem., 184 (1980) 379.

[20] S. Greulich, R. Reinhardt and W. Kaim, unpublished results.
[21] J.A. Weil, J.R. Bolton and J.E. Wertz, Electron Paramagnetic Resonance, Wiley, New York, 1994.
[22] N.S. Hosmane, Y. Wang, H. Zhang, J.A. Maguire, E. Waldhör and W. Kaim, Organometallics, 12 (1993) 3785.
[23] T.A. Albright, W.E. Geiger, Jr., J. Moraczewski and B. Tulyathan, J. Am. Chem. Soc., 103 (1981) 4787.
[24] M. Krejcik, M. Danek and F. Hartl, J. Electroanal. Chem., 317 (1991) 179.
[25] A.B.P. Lever Inorganic Electronic Spectroscopy, Elsevier, Amsterdam, 1984.
[26] W. Kaim, R. Reinhardt and M. Sieger, Inorg. Chem., 33 (1994) 4453.
[27] W.A. Fordyce and G.A. Crosby, Inorg. Chem., 21 (1982) 1023.
[28] E. König and S. Kremer, Chem. Phys. Lett., 5 (1970) 87.
[29] W. Bruns, W. Kaim, E. Waldhör and M. Krejcik, Inorg. Chem., 34 (1995) 663.
[30] U. Kölle, F. Khouzami and B. Fuss, Angew. Chem. Suppl., (1982) 230.
[31] W. Kaim, S. Ernst and V. Kasack, J. Am. Chem. Soc., 112 (1990) 173.